IET Generation, Transmission & Distribution

Special Issue: Optimal Utilisation of Storage Systems in Transmission and Distribution Systems

IET Journals
The Institution of Engineering and Technology

Optimal scheduling of virtual power plant with battery degradation cost

ISSN 1751-8687
Received on 27th January 2015
Revised on 18th June 2015
Accepted on 22nd June 2015
doi: 10.1049/iet-gtd.2015.0103
www.ietdl.org

Bin Zhou[1], Xi Liu[1], Yijia Cao[1], Canbing Li[1] ✉, Chi Yung Chung[2], Ka Wing Chan[3]

[1]College of Electrical and Information Engineering, Hunan University, Changsha 410082, People's Republic of China
[2]Department of Electrical and Computer Engineering, University of Saskatchewan, Canada
[3]Department of Electrical Engineering, The Hong Kong Polytechnic University, Hong Kong
✉ E-mail: licanbing@qq.com

Abstract: This study proposes a novel optimal generation scheduling model for virtual power plant (VPP) considering the degradation cost of energy storage system (ESS). The VPP is generally formed by a mix of distributed energy resources, and the ESS is an important installation for flexible VPP dispatch due to its controllable and schedulable behaviours. For the operations of battery storage systems, the ambient temperature and depth of discharge have significant impacts on the wear and tear of the ESS as well as battery degradation cost. Furthermore, the battery degradation cost is modelled and approximated by a piecewise linear function, and then incorporated into the proposed optimal VPP scheduling model. Consequently, the optimal VPP scheduling problem is formulated as a two-stage stochastic mixed-integer linear programming in order to maximise the expected profits of the VPP. The proposed model has been successfully implemented and tested through a representative case study, and the influence of battery degradation cost on optimal VPP scheduling has also been thoroughly analysed and demonstrated.

Nomenclature

Acronyms

BEV	battery electric vehicle
CTPP	conventional thermal power plant
CVaR	conditional value at risk
DoD	depth of discharge
ESS	energy storage system
EV	electric vehicle
MILP	mixed-integer linear programming
PHEV	plug-in hybrid EV
PV	photovoltaic
VPP	virtual power plant
WPP	wind power plant

Sets

B	sets of batteries
P	sets of day-ahead market price scenarios
S	sets of PV power output scenarios
W	sets of WPP power output scenarios
T	sets of time periods

Constants

$g_{b,0}$	initial energy stored in battery b (MWh)
$g_{b\max}$	maximum capacity of battery b (MWh)
$g_{b\min}$	minimum capacity of battery b (MWh)
$g^{\mathrm{c}}_{\max}$	maximum power output of the CTPP (MW)
$g^{\mathrm{c}}_{\min}$	minimum power output of the CTPP (MW)
$g_{s,t}$	PV power output in time period t and PV power output scenario s (MW)
$g_{w,t}$	WPP power output in time period t and WPP power output scenario w (MW)
$L^{\min}_{\mathrm{down}}$	constant equals to min $[T, (T^{\min}_{\mathrm{down}} - T^{\mathrm{init}}_{\mathrm{down}}) \cdot (1 - T^{\mathrm{off}}_{\mathrm{on}})]$, which is the number of time periods that the CTPP has to be down from the beginning of the planning horizon (h)
$L^{\min}_{\mathrm{up}}$	constant equals to min $[T, (T^{\min}_{\mathrm{up}} - T^{\mathrm{init}}_{\mathrm{up}}) \cdot T^{\mathrm{off}}_{\mathrm{on}}]$, which is the number of time periods that the CTPP has to be up from the beginning of the planning horizon (h)
ru	ramp-up limit of the CTPP (MW/h)
rd	ramp-down limit of the CTPP (MW/h)
S_{c}	start-up cost of CTPP (€)
$T^{\mathrm{init}}_{\mathrm{down}}$	the number of time periods that the CTPP has been down before the beginning of the planning horizon (h)
$T^{\min}_{\mathrm{down}}$	minimum-down time of the CTPP (h)
$T^{\mathrm{off}}_{\mathrm{on}}$	CTPP on–off status before the beginning of the planning horizon (equals to 1 if $T^{\mathrm{init}}_{\mathrm{up}} > 0$, and 0 otherwise)
$T^{\mathrm{init}}_{\mathrm{up}}$	the number of time periods that the CTPP has been up before the beginning of the planning horizon (h)
$T^{\min}_{\mathrm{up}}$	maximum-up time of the CTPP (h)
δ^{+}_{b}	maximum energy can be charged to battery b during one period (MWh)
δ^{-}_{b}	maximum energy can be discharge from battery b during one period (MWh)
η^{+}_{b}	charge efficiency of battery b
η^{-}_{b}	discharge efficiency of battery b
φ_{down}	down-regulation price ratio
φ_{up}	up-regulation price ratio
$\lambda_{\mathrm{p},t}$	electricity price in the day-ahead market in time period t and day-ahead market price scenario p (€/MWh)
π_p	probability of the pth day-ahead market price scenario
π_s	probability of the sth PV power output scenario
π_w	probability of the wth WPP power output scenario

Variables

$C^{\mathrm{C}}_{w,s,p,t}$	fuel cost of the CTPP (€)
$C^{B}_{w,s,p,b,t}$	degradation cost of battery b (€)
$g_{w,s,p,b,t}$	energy stored in battery b at the end of time period t (MWh)
$g^{+}_{w,s,p,b,t}$	energy charged to battery b during time period t (MWh)

$g^{-}_{w,s,p,b,t}$	energy discharged from battery b during time period t (MWh)
$g^{c}_{w,s,p,t}$	CTPP power output (MW)
$g^{down}_{w,s,p,t}$	electricity sold in the balancing market (MW)
$g^{up}_{w,s,p,t}$	electricity purchased in the balancing market (MW)
$G_{w,s,p,b,t}$	electricity sold (positive) or purchased (negative) in the day-ahead market (MW)
$u_{w,s,p,b,t}$	binary variable equals to 1 if battery b is charged, and 0 otherwise
$v_{w,s,p,b,t}$	binary variable equals to 1 if battery b is discharged, and 0 otherwise
$x_{w,s,p,t}$	binary variable equals to 1 if the CTPP is on, and 0 otherwise
$y_{w,s,p,t}$	binary variable equals to 1 if the CTPP is started up at the beginning of the time period, and 0 otherwise
ζ	auxiliary variable for computing the CVaR (€)
$\eta_{w,s,p}$	auxiliary variable for computing the CVaR (€)

1 Introduction

Renewable energy technologies have caught great attention in recent years because of the growing environmental consciousness. Various investment and incentive schemes in this field have been carried out worldwide, especially in wind power and photovoltaic (PV) generations [1, 2]. However, the inherent fluctuation and volatility characteristics of wind power and PV generations have brought significant instability to power systems and the profit obtained by individual agents is usually lower than some other advanced energy generations. Besides, it is risky for the owners of wind power plants (WPPs) and PV plants to trade in electricity markets since the imbalance costs are inevitable and the incentive schemes are not desirable within a contracted time limit [3, 4]. Consequently, renewable energy sources, energy storage systems (ESSs), and dispatchable power plants are combined to form a single virtual power plant (VPP). This unique aggregation not only can overcome the uncertainties of intermittent renewable generations and improve the power quality, but also enable the VPP agent to make more profits. Studies on the collaborative scheduling optimisation, risk aversion, and the ESS utilisation have been investigated for VPP management in recent years [5–9].

The main goal for a VPP agent is to optimise the scheduling and make profit. A short-term offering model for a VPP based on stochastic programming was presented in [10] to maximise its expected profit in both the day-ahead and balancing electricity markets. Considering the long-term bilateral contracts, Pandžić *et al.* [11] proposed a VPP model containing a pumped hydro storage plant to optimise the profit. Nevertheless, the risk of actual profit is not tackled in the aforementioned studies, and thus the conditional value at risk (CVaR) was applied as a risk evaluation technique for a VPP model to lower the risk of low profit scenarios in electricity markets [12]. With a weighted CVaR, a coordinated trading of WPP and conventional thermal power plant (CTPP) was presented in [13], which significantly improves the expected profits in the lowest lucrative scenarios. Electric vehicles (EVs) have received significant attention as an emerging energy storage form for the VPP. An agent-based approach was presented in [14] to increase the profit of the VPP with a special payment for EVs participation. In order to analyse the cost and emission impacts caused by plug-in hybrid EVs (PHEVs) application in the VPP, Arslan and Karasan [15] developed an energy management model for a VPP including PHEVs and distributed energy resources.

Although it is convenient and clean to use EV batteries as the ESS for a VPP, the battery lifespan limitation and wear and tear caused by frequent charging and discharging will bring remarkable impacts on VPP scheduling with EV batteries. An optimal control strategy was proposed in [16] for PHEV battery fleets to maximise the efficiency of the power-train as well as minimise the battery degradation cost. Furthermore, the correlations among charging/discharging patterns, depth of discharge (DoD), ambient temperature, and the degradation cost of battery EV (BEV) batteries were formulated in [17] on the basis of rigorous mathematical analysis. Numerical results show that DoD and ambient temperature are two important factors which can cause considerable degradation cost to BEV batteries.

So far, the influence of battery degradation cost on the optimal VPP scheduling in the day-ahead and balancing markets has not yet been studied. It is obvious that a battery has a limited lifespan, namely a cycle life, due to its inherent physical and chemical characteristics [18]. Factors, such as DoD, ambient temperature, and high discharge currents play crucial roles in shortening the battery cycle life [19, 20], and thus lead to an inevitable cost to VPP participation. Although the degradation cost of a single battery can be negligible for simplicity, for a VPP comprising plenty of batteries, the degradation cost has a significant impact on the overall expected profit. Therefore, it is worth modelling the battery degradation cost in the VPP scheduling problem. Concerning the reviewed work, the main contribution of this paper is to incorporate the battery degradation cost into the proposed model and in-depth analysis of the effects of battery degradation cost on the VPP scheduling.

A novel optimal scheduling model for a VPP is proposed in this paper. The battery fleets are used as the energy storage medium not only to compensate the fluctuation of WPP and PV generations, but also to provide optimal operations to maximise the expected profit. Using piecewise linearisation methods, the VPP model with battery degradation cost, uncertain renewable generations, and market price is formulated as a two-stage stochastic mixed-integer linear programming (MILP).

2 Problem formulation

2.1 Uncertainty modelling

Both the day-ahead and the balancing markets are considered in this paper to provide flexible electricity trade for a VPP operator. The VPP submits bids/offers to the day-ahead market for several hours (usually 10–14 h) prior to the operation hour. The balancing market enables the VPP operator to purchase or sell electricity close to real time for regulating energy deviations caused by uncertain WPP and PV generations. Following current practice in European power market, a dual pricing scheme is provided for the VPP operator to purchase electricity in the balancing market at a price higher than that in the day-ahead market (up-regulation), and sell electricity in the balancing market at a price lower than that in the day-ahead market (down-regulation) [10, 12].

The VPP model consists of a WPP, a PV power plant, a CTPP, and the battery fleets. Since there are uncertainties in day-ahead market price, WPP and PV generations, it is important to predict them accurately for optimal scheduling of the VPP. Investigations on uncertainty prediction techniques of these uncertainties are abundant and fruitful [21–25]. In this paper, the historical data are used to form scenarios with equal probability of occurrence for modelling uncertainties [10, 11].

A classical two-stage stochastic programming is used to tackle the aforementioned uncertainties [26, 27]. In the first stage, the VPP operator should make decisions on the amount of sold/purchased electricity in the day-ahead market, before all the uncertainties become known (here-and-now decisions). In the second stage, the VPP operator should decide the operations of the CTPP and battery fleets after the revelation of uncertainties (wait-and-see decisions). The goal of the VPP operator is to maximise the expected profit. A top-level flowchart of the two-stage stochastic programming is shown in Fig. 1.

2.2 Battery degradation cost

Battery fleets are utilised in the VPP not only to tackle the intermittent renewable generations, but also to enable the VPP operator to sell electricity with high market prices. Several factors contribute to the battery degradation cost, while most of the previously reported studies only consider the DoD in the

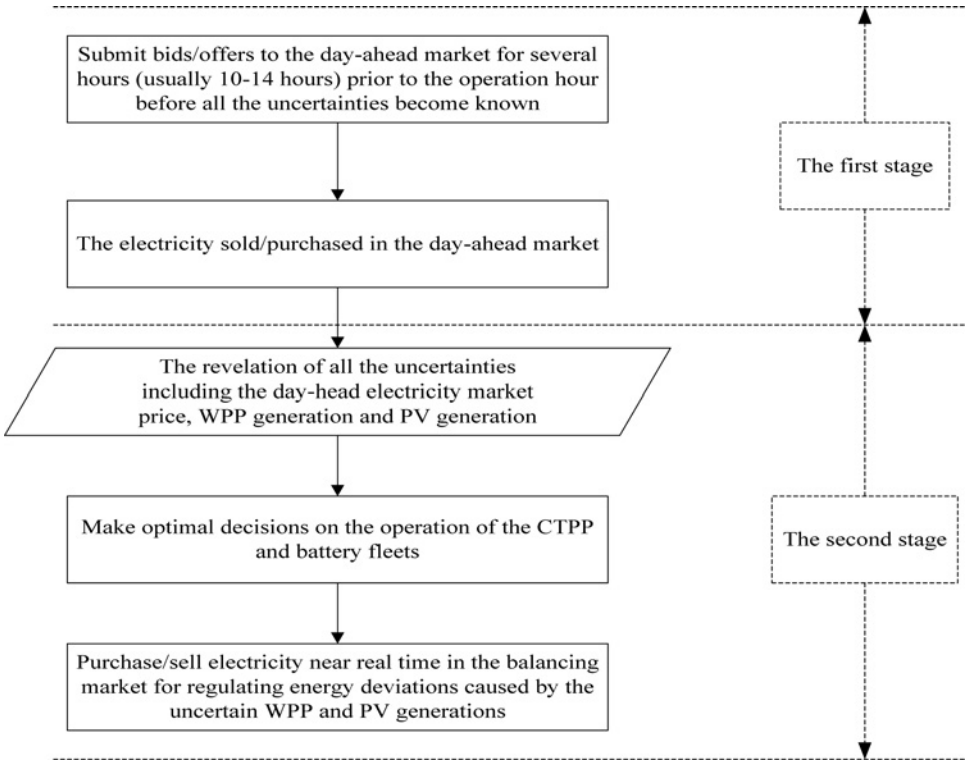

Fig. 1 *Top-level flowchart of the two-stage stochastic programming*

scheduling problems. Consequently, the DoD combined with ambient temperature is taken into account to model the battery degradation cost.

Among the studies on battery degradation cost modelling [17, 28–30], this paper adopts the methods proposed in [17, 28], in which the battery degradation cost is formulated as the wear and tear for VPP participation due to the extra cycling under extreme ambient temperature and the change in DoD during charging/discharging periods. Besides, additional thermal management system and DoD deviation control aggregator are necessary in battery life regulation [31]. In this paper, the worst case that none of them are implemented is studied for better understanding the effect of battery degradation cost on optimal VPP scheduling.

In this paper, the DoD can be formulated as follows

$$\mathrm{DoD} = 1 - \frac{g_v}{g_{v\max}} \tag{1}$$

where g_v is the energy stored in the battery; and $g_{v\max}$ is the maximum energy capacity of battery [15].

The studied battery fleets include lead-acid batteries and nickel metal hydride (NiMH) batteries. Using the data points provided by the manufacturer, the correlations between DoD and cycle life of the two types of batteries can be obtained using MATLAB curve fitting tools and expressed by (2) and (3), respectively,

$$L_{\text{lead-acid}} = a\mathrm{DoD}_{\text{lead-acid}} + b \tag{2}$$

where a and b are coefficients of cycle life dependence on DoD; $L_{\text{lead-acid}}$ and $\mathrm{DoD}_{\text{lead-acid}}$ are cycle life in the number of cycles and DoD of the lead-acid battery, respectively. Here, $a = -4230$ and $b = 4332$

$$L_{\text{NiMH}} = \beta_0\left(\frac{\mathrm{DoD}_{\text{ref}}}{\mathrm{DoD}_{\text{NiMH}}}\right)^{\beta_1}\exp\left(\beta_2\left(1 - \frac{\mathrm{DoD}_{\text{NiMH}}}{\mathrm{DoD}_{\text{ref}}}\right)\right) \tag{3}$$

where β_0, β_1, and β_2 are coefficients of cycle life dependence on DoD; $\mathrm{DoD}_{\text{ref}}$, L_{R}, $\mathrm{DoD}_{\text{NiMH}}$, and L_{NiMH} are the rated DoD, rated cycle life, DoD, and cycle life of the NiMH battery, respectively. In this paper, $\beta_0 = 1400$, $\beta_1 = 0.886$, and $\beta_2 = -0.3997$ were obtained from the curve fitting results.

The correlations between ambient temperature and cycle life for the two types of batteries can be obtained from experimental data and curve fitting method, as shown in (4) and (5), respectively,

$$L_{\text{lead-acid}} = k\exp(\alpha T) \tag{4}$$

where k and α are coefficients of cycle life dependence on the temperature; $L_{\text{lead-acid}}$ and T are cycle life in the number of cycles of the lead-acid battery and ambient temperature in degree centigrade, respectively. In this paper, $k = 3291$ and $\alpha = -0.05922$

$$L_{\text{NiMH}} = aT^3 + bT^2 + cT + d \tag{5}$$

where a, b, c, and d are coefficients of cycle life dependence on temperature; L_{NiMH} and T are cycle life in the number of cycles of the NiMH battery and ambient temperature in degree centigrade, respectively. In this paper, $a = 0.002424$, $b = 0.4879$, $c = 6.742$, and $d = 1524$.

As an example, the correlations among ambient temperature and cycle life, DoD and cycle life of the NiMH battery are presented in Figs. 2*a* and *b*, respectively. As shown in the figures, the cycle life is inversely proportional with both DoD and ambient temperature. In other words, deep discharging and high ambient temperature can notably shorten the cycle life. It is important to note that the cycle life reduces more with the increase of DoD than that of temperature.

Using the model proposed by Kempton and Tomić [28], the degradation cost C_v is defined as

$$C_v = \frac{C_b}{L_N \cdot E_v \cdot \mathrm{DoD}_{\text{ref}}} \tag{6}$$

where C_b is the battery capital cost in € considering replacement labour; L_N is the battery lifespan in the number of cycles; E_v is the total energy storage of the battery in kWh, and $\mathrm{DoD}_{\text{ref}}$ is the

IET Gener. Transm. Distrib., 2016, Vol. 10, Iss. 3, pp. 712–725

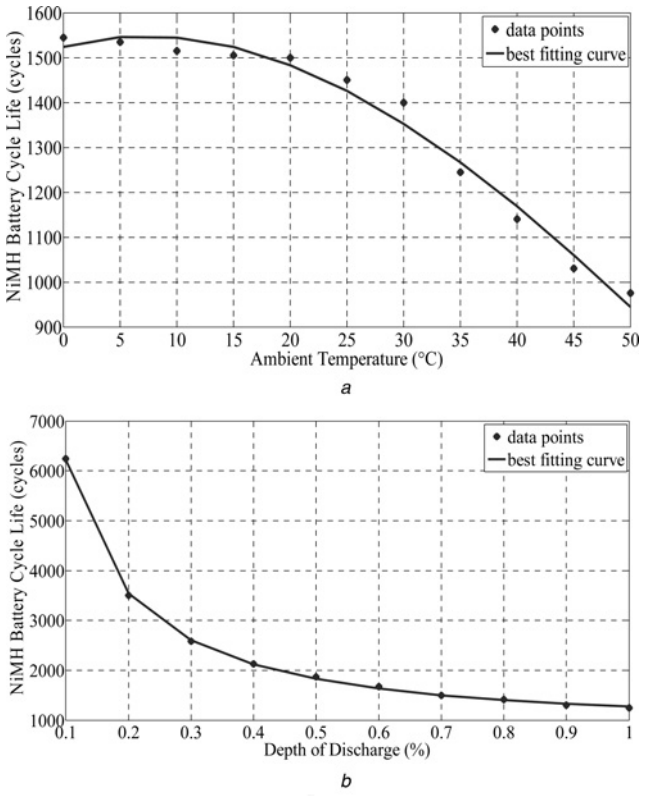

Fig. 2 *Correlations among DoD, ambient temperature, and cycle life of the NiMH battery*

a Correlation between ambient temperature and cycle life of the NiMH battery
b Correlation between DoD and cycle life of the NiMH battery

reference DoD. L_N and E_v can be calculated under a reference condition (ambient temperature $T = 20^{\circ}$C, $\mathrm{DoD}_{\mathrm{ref}} = 80\%$).

In this paper, the overall effect of ambient temperature and DoD on the battery lifespan is defined as

$$L_{\mathrm{VPP}} = \frac{L_{\mathrm{ATEM}} \cdot L_{\mathrm{ADoD}}}{L_{\mathrm{R}}} \tag{7}$$

where L_{VPP} is the battery lifespan with VPP participation; L_{R} is the rated battery cycle life estimated by manufactures under rated ambient temperature and DoD; L_{ATEM} and L_{ADoD} are the actual cycle life of a battery, respectively, which can be acquired from (2)–(5).

Hence, the battery degradation cost with VPP participation considering the overall effect of ambient temperature and DoD can be expressed as

$$C_{\mathrm{VPP}} = \frac{C_b}{L_{\mathrm{VPP}} \cdot E_v \cdot \mathrm{DoD}_{\mathrm{ref}}} \tag{8}$$

The degradation cost of lead-acid battery can be obtained from (2), (4), (7), and (8), which is defined by

$$C_{\mathrm{VPP}}^{\text{lead-acid}} = \frac{C_b \cdot L_{\mathrm{R}}}{k \cdot (a\mathrm{DoD}_{\text{lead-acid}} + b) \cdot \exp(\alpha T) \cdot E_v \cdot \mathrm{DoD}_{\mathrm{ref}}} \tag{9}$$

Moreover, the degradation cost of NiMH battery can be obtained from (3), (5), (7), and (8), which is presented by (see (10))

2.3 Formulation

The objective function of optimal VPP scheduling model with battery degradation cost is formulated as follows (see (11))

subject to

$$x_{w,s,p,t} - x_{w,s,p,t-1} \le y_{w,s,p,t}, \quad \forall w \in n_w, \forall s \in n_s, \forall p \in n_p, \forall t \in T \tag{12}$$

$$g^{\mathrm{c}}_{\min} \cdot x_{w,s,p,t} \le g^{\mathrm{c}}_{w,s,p,t} \le g^{\mathrm{c}}_{\max} \cdot x_{w,s,p,t}, \quad \forall w \in n_w, \forall s \in n_s, \forall p \in n_p, \forall t \in T \tag{13}$$

$$-\mathrm{rd} \le g^{\mathrm{c}}_{w,s,p,t} - g^{\mathrm{c}}_{w,s,p,t-1} \le ru, \quad \forall w \in n_w, \forall s \in n_s, \forall p \in n_p, \forall t \in T \tag{14}$$

$$\sum_{t=1}^{L^{\min}_{\mathrm{down}}} x_{w,s,p,t} = 0, \quad \forall w \in n_w, \forall s \in n_s, \forall p \in n_p \tag{15}$$

$$\sum_{t'=t}^{t+T^{\min}_{\mathrm{down}}-1} (1 - x_{w,s,p,t'}) \ge T^{\min}_{\mathrm{down}} \cdot (x_{w,s,p,t-1} - x_{w,s,p,t}), \quad \forall w \in n_w, \forall s \in n_s, \forall p \in n_p, \quad \forall t \in [L^{\min}_{\mathrm{down}} + 1, T - T^{\min}_{\mathrm{down}} + 1] \tag{16}$$

$$\sum_{t'=t}^{T} [1 - x_{w,s,p,t'} - (x_{w,s,p,t-1} - x_{w,s,p,t})] \ge 0, \quad \forall w \in n_w, \forall s \in n_s, \forall p \in n_p, \forall t \in [T - T^{\min}_{\mathrm{down}} + 2, T] \tag{17}$$

$$\sum_{t=1}^{L^{\min}_{\mathrm{up}}} (1 - x_{w,s,p,t}) = 0, \quad \forall w \in n_w, \forall s \in n_s, \forall p \in n_p \tag{18}$$

$$\sum_{t'=t}^{t+T^{\min}_{\mathrm{up}}-1} x_{w,s,p,t'} \ge T^{\min}_{\mathrm{up}} \cdot y_{w,s,p,t}, \quad \forall w \in n_w, \forall s \in n_s, \forall p \in n_p, \forall t \in [L^{\min}_{\mathrm{up}} + 1, T - T^{\min}_{\mathrm{up}} + 1] \tag{19}$$

$$\sum_{t'=t}^{T} (x_{w,s,p,t} - y_{w,s,p,t})] \ge 0, \quad \forall w \in n_w, \forall s \in n_s, \forall p \in n_p, \forall t \in [T - T^{\min}_{\mathrm{up}} + 2, T] \tag{20}$$

$$g_{b\min} \le g_{w,s,p,b,t} \le g_{b\max}, \quad \forall w \in n_w, \forall s \in n_s, \forall p \in n_p, \forall b \in B, \forall t \in T \tag{21}$$

$$C_{\mathrm{VPP}}^{\mathrm{NiMH}} = \frac{C_b \cdot L_{\mathrm{R}}}{\beta_0 \cdot (\mathrm{DoD}_{\mathrm{ref}}/\mathrm{DoD}_{\mathrm{NiMH}})^{\beta_1} \cdot \exp\big(\beta_2 \cdot (1 - (\mathrm{DoD}_{\mathrm{NiMH}}/\mathrm{DoD}_{\mathrm{ref}}))\big) \cdot (aT^3 + bT^2 + cT + d) \cdot E_v \cdot \mathrm{DoD}_{\mathrm{ref}}} \tag{10}$$

$$\max \sum_{t \in T} \sum_{w \in n_w} \pi_w \cdot \sum_{s \in n_s} \pi_s \cdot \sum_{p \in n_p} \pi_p \cdot [\lambda_{p,t} \cdot (G_{w,s,p,t} + g^{\mathrm{down}}_{w,s,p,t} \cdot \varphi_{\mathrm{down}} - g^{\mathrm{up}}_{w,s,p,t} \cdot \varphi_{\mathrm{up}}) - C^{\mathrm{C}}_{w,s,p,t} - y_{w,s,p,t} \cdot S_{\mathrm{c}} - C^{\mathrm{B}}_{w,s,p,b,t}] \tag{11}$$

$$g_{w,s,p,b,0} = g_{b,0}, \quad \forall w \in n_w, \forall s \in n_s, \forall p \in n_p, \forall b \in B, \forall t \in T \tag{22}$$

$$u_{w,s,p,b,t} + v_{w,s,p,b,t} \le 1, \quad \forall w \in n_w, \forall s \in n_s, \forall p \in n_p, \forall b \in B, \forall t \in T \tag{23}$$

$$0 \le g^{+}_{w,s,p,b,t} \le \delta^{+}_{b} \cdot u_{w,s,p,b,t}, \quad \forall w \in n_w, \forall s \in n_s, \forall p \in n_p, \forall b \in B, \forall t \in T \tag{24}$$

$$0 \le g^{-}_{w,s,p,b,t} \le \delta^{-}_{b} \cdot v_{w,s,p,b,t}, \quad \forall w \in n_w, \forall s \in n_s, \forall p \in n_p, \forall b \in B, \forall t \in T \tag{25}$$

$$g_{w,s,p,b,t} = g_{w,s,p,b,t-1} + \eta^{+}_{b} \cdot g^{+}_{w,s,p,b,t} - \frac{1}{\eta^{-}_{b}} \cdot g^{-}_{w,s,p,b,t}, \quad \forall w \in n_w, \forall s \in n_s, \forall p \in n_p, \forall b \in B, \forall t \in T \tag{26}$$

$$g^{\mathrm{c}}_{w,s,p,t} + g_{w,t} + g_{s,t} + g^{\mathrm{up}}_{w,s,p,t} + \sum_{b \in B} g^{-}_{w,s,p,b,t} = G_{w,s,p,t} + g^{\mathrm{donw}}_{w,s,p,t} + \sum_{b \in B} g^{+}_{w,s,p,b,t} \quad \forall w \in n_w, \forall s \in n_s, \forall p \in n_p, \forall b \in B, \forall t \in T \tag{27}$$

$$G_{1,1,p,t} = G_{1,2,p,t} \cdots = G_{2,2,p,t} \cdots = G_{n_w,n_s,p,t}, \quad \forall p \in n_p, \forall t \in T \tag{28}$$

$$x_{w,s,p,t}, y_{w,s,p,t}, u_{w,s,p,b,t}, v_{w,s,p,b,t} \in \{0, 1\}, \quad \forall w \in n_w, \forall s \in n_s, \forall p \in n_p, \forall b \in B, \forall t \in T \tag{29}$$

In the above formulation, the expected profit of the VPP is maximised by the objective function (11) which includes electricity sold/purchased in the day-ahead market ($G_{w,s,p,t}$), sold in the down-regulation balancing market ($g^{\mathrm{down}}_{w,s,p,t}$), and purchased in the up-regulation balancing market ($g^{\mathrm{up}}_{w,s,p,t}$), as well as the fuel cost ($C^{\mathrm{C}}_{w,s,p,t}$) and start-up cost ($y_{w,s,p,t} \cdot S_{\mathrm{c}}$) of the CTPP and the battery degradation cost ($C^{\mathrm{B}}_{w,s,p,b,t}$). Here, φ_{up} and φ_{down} are up-regulation price ratio and down-regulation price ratio, respectively. In this paper, $\varphi_{\mathrm{up}} = 1.3$ and $\varphi_{\mathrm{down}} = 0.7$.

Constraints of the CTPP are presented in (12)–(20). Constraint (12) denotes the correlation between binary $x_{w,s,p,t}$ and $y_{w,s,p,t}$. $x_{w,s,p,t}$ equals to 1 if the CTPP is on, and 0 otherwise. $y_{w,s,p,t}$ equals to 1 if the CTPP is started up, and 0 otherwise. Constraint (13) presents the minimum and maximum power output limits of the CTPP. Constraint (14) enforces the ramp rate limits. Minimum-down time constraints are expressed in (15)–(17), indicating that if the CTPP is switched off, it has to remain off for $T^{\mathrm{min}}_{\mathrm{down}}$ hours. Constraint (15) enforces the CTPP to stay off for $L^{\mathrm{min}}_{\mathrm{down}}$ hours if the CTPP has already been off at hour 0. Then, the minimum-down time constraint for all combinations of consecutive hours of size $T^{\mathrm{min}}_{\mathrm{down}}$ is enforced by constraint (16). Constraint (17) is used to meet the minimum-down time constraint for the last $T^{\mathrm{min}}_{\mathrm{down}} - 1$ h. Constraints (18)–(20) enforce the minimum-up time constraint in a similar manner as described above.

Constraints (21)–(26) are related to the battery fleets. Constraint (21) enforces the minimum and maximum energy storage limits for each battery. The initial energy stored in each battery is stated by constraint (22). Constraint (23) describes the fact that charging and discharging cannot be done simultaneously. $u_{w,s,p,b,t}$ and $v_{w,s,p,b,t}$ are binary variables. $u_{w,s,p,b,t}$ equals to 1 if battery b is charged, and 0 otherwise. $v_{w,s,p,b,t}$ equals to 1 if battery b is discharged, and 0 otherwise. Constraints (24) and (25) enforce the maximum charging and discharging powers of each battery, respectively. Constraint (26) declares the energy stored in each battery between two consecutive periods. η^{+}_{b} and η^{-}_{b} are the charging and discharging efficiencies of each battery, respectively.

Constraint (27) is the energy balance equality constraint. It indicates that the electricity generated by CTPP, WPP, and PV power plant, plus the electricity purchased in the balancing market and the electricity discharged from battery fleets, equals to the electricity sold ($G_{w,s,p,t} \ge 0$), or purchased ($G_{w,s,p,t} \le 0$) in the day-ahead market plus the electricity sold to the balancing market and the electricity charged to battery fleets. Constraint (28) denotes that $G_{w,s,p,t}$ is only related to the time and day-ahead market prices, ensuring that only one bidding curve is submitted to the day-ahead market in each hour, irrespective of the WPP and PV power outputs. Finally, binary variables are defined by constraint (29). This model guarantees a flexible operation for the CTPP and the battery fleets to meet the realisation of various scenarios.

3 Case studies

In this paper, the operator aims to find the optimal scheduling decisions for a VPP considering battery degradation cost. A WPP, a PV power plant, a CTPP, and the battery fleets are combined to form the VPP.

3.1 Simulation environment

The considered time horizon is 24 h, and the characteristics of the CTPP are shown in Table 1. In order to linearise the model, a 2-block piecewise linear function is used to approximate the quadratic CTPP fuel cost function. It is assumed that the CTPP has been shut up for 1 h (i.e. $T^{\mathrm{init}}_{\mathrm{down}} = 1$) before the considered time horizon.

Five equiprobable WPP power output scenarios based on historical data are shown in Fig. 3*a*. These data are obtained from a WPP with a rated capacity of 10.2 MW, located in Weybourne, Norfolk coast area of the UK. Fig. 3*b* presents five equiprobable power output scenarios of a PV power plant with a rated capacity of 10 MW. They are formed using historical data collected from EEX transparency platform [32]. Fig. 3*c* shows five equiprobable day-ahead market price scenarios based on real data obtained from APX Power UK [33].

Table 2 shows the characteristics of the two studied batteries. The correlations among degradation cost, DoD, and ambient temperature of the lead-acid battery are presented in Figs. 4*a* and *b* is related to NiMH battery. As shown in the two figures, degradation cost increases with rising ambient temperature and DoD due to the reduction of cycle life. Besides, the degradation cost of NiMH battery is lower comparing with that of lead-acid battery in the same ambient temperature and DoD. Figs. 4*c* and *d* show the correlation between degradation cost and DoD of the lead-acid battery and NiMH battery under different ambient temperatures, respectively. The two figures indicate that with the same DoD, high ambient temperature causes high degradation cost. Besides, degradation cost increases logarithmically with the increase of DoD for the lead-acid battery but exponentially for the NiMH battery. Piecewise linear functions are used to fit the non-linear degradation cost function in order to keep the linearity of this model [15]. Battery fleets in this paper are composed of 500 lead-acid batteries (battery fleet *a*) and 500 NiMH batteries (battery fleet *b*), thus the maximum and minimum capacities of the battery fleets are 28.935 and 3.215 MWh, respectively. It is assumed that the initial energy storage of the battery fleets is

Table 1 CTPP data

a, MBtu/MW^{2}h	*b*, MBtu/MWh	*c*, MBtu	Start-up fuel, MBtu	Fuel price, €/MBtu	P_{max}, MW	P_{min}, MW	Min-up, h	Min-down, h	ramp, MW/h
0.0029	6.05	40.53	20.14	1	16	3.5	3	3	5

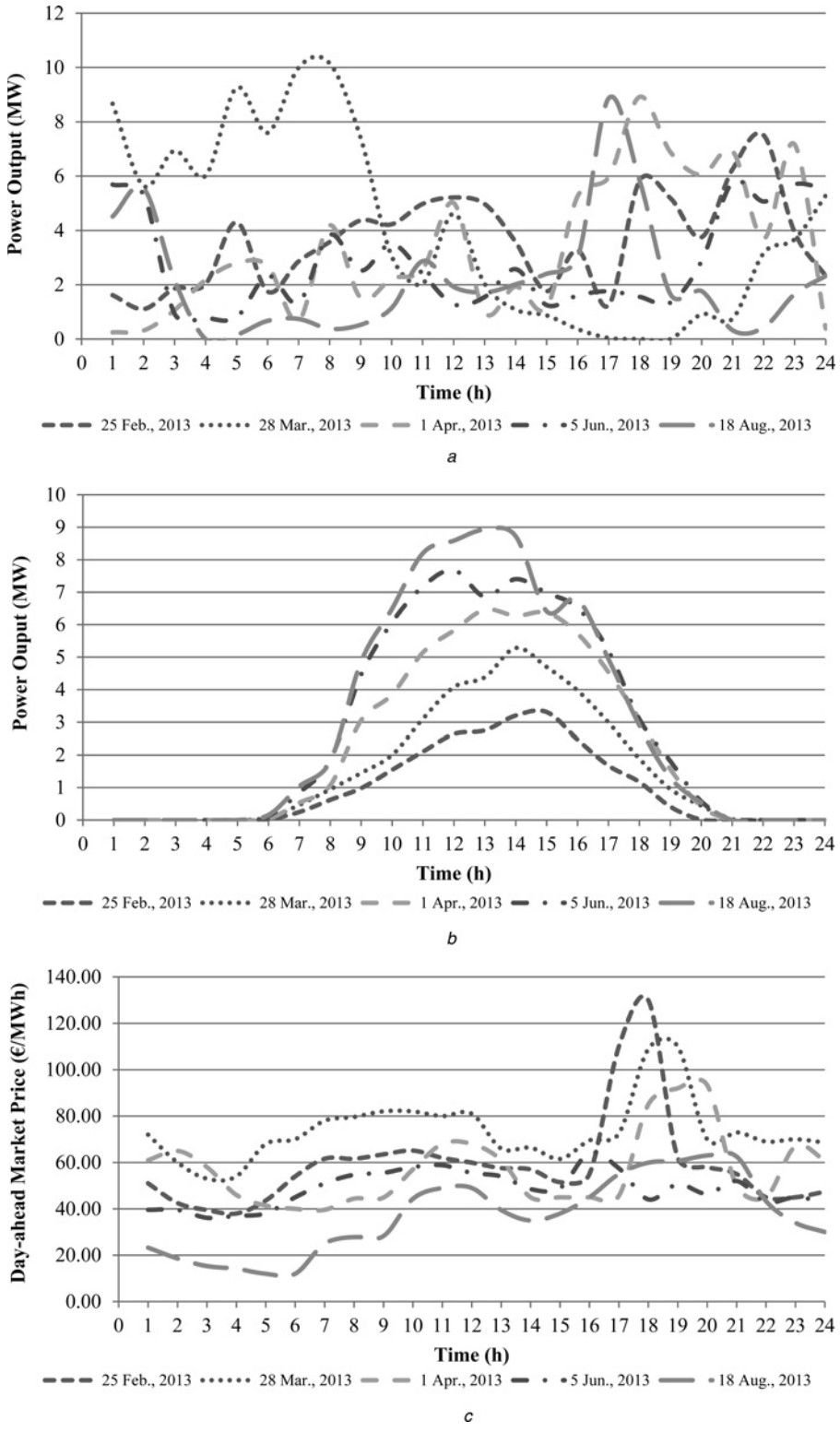

Fig. 3 *Five WPP power output, five PV plant power output, and day-ahead market price scenarios*

a Five WPP power output scenarios
b Five PV plant power output scenarios
c 5 day-ahead market price scenarios

3.215 MW. In this paper, the degradation cost is counted only when the battery fleets are operated by the VPP operator.

3.2 Computational results

Assuming the ambient temperature is 20°C, Fig. 5 presents the expected hourly and cumulative profit of the VPP together with the hourly and cumulative degradation cost in case 1 (with battery degradation cost) and case 2 (without battery degradation cost). In hour 1, the initial energy stored in the battery fleets is discharged to sell in the day-ahead market in case 2. While in case 1, no electricity is discharged from the battery fleets to avoid the degradation cost, resulting in lower profit than case 2. Since the day-ahead market prices are the lowest in the following 4 h, the electricity produced by the VPP is used to charge the battery fleets

Table 2 Battery data

Characteristics	Lead-acid battery	NiMH battery
rated capacity, kWh	28.3	36
maximum capacity, kWh[a]	25.47	32.4
minimum capacity, kWh[a]	2.83	3.6
initial energy storage, kWh	2.83	3.6
maximum charging/discharging power, kWh[a]	5.66	7.2
charging/discharging efficiency, %	91.4	92.5
rated DoD, %	80	70
capital cost, €	2716.8	4032
cycle life, cycles[b]	1000	1500

[a]For prolonging battery lifespan, the maximum and minimum capacities are set to be 90 and 10% of the rated capacity, respectively. Additionally, the maximum charging/discharging power could not exceed 20% of the rated capacity [14].
[b]Assuming the ambient temperature is 20°C.

in both of the two cases. From hours 6 to 24, the hourly profits vary by the day-ahead market prices. In other words, electricity produced by the VPP is sold in the day-ahead market when the market prices are high but used to charge the battery fleets when the market prices are low. Comparing to case 2, the profits in most of these hours are lower in case 1 due to the degradation cost. In hours 2, 4, 5, 14, 15, 16, and 22, the profits in case 1 are higher than case 2, because the VPP operator chooses to charge the battery fleets during these hours in case 2 while sells electricity to day-ahead market in case 1 for averting the degradation cost. Besides, the degradation cost in hours 3, 8, 12, 15, and 21 increases owning to the fact that market prices start to fall during these hours and battery fleets are used to store the electricity. The highest profits of both the two cases are acquired in hour 18 because of the highest market prices in most scenarios. The expected daily profit of the VPP is 23 841.65 € but falls to 20 839.87 € (i.e. a 12.59% reduction) when battery degradation cost is counted. It is worth to note that the overall degradation cost throughout the day is 779.17 € which is not the difference between the expected daily profits of the two cases. Hence the degradation cost has significant impacts on the optimal VPP decisions, which will be illustrated in the following sections.

Electricity sold in the day-ahead market for different market price scenarios in the two cases is shown in Figs. 6*a* and *b*, respectively. As shown from Fig. 6*a*, electricity sold in hour 5 is higher than that of the contiguous few hours, since the CTPP starts to generate power with its maximum capacity in hour 5. While in the following few hours, electricity is used to charge the battery fleets. It is important to note that for all scenarios in case 1, the largest amount of electricity is sold in hour 16 rather than in hour 18 which exhibits the highest market price. This is because the market price begins to rise from hour 16 in most of the scenarios, and thus the battery fleets are fully discharged for selling electricity in the day-ahead market, causing a significant increase of DoD as well as the battery degradation cost. As a result, the VPP operator tries to discharge less electricity from the battery fleets in order to realise optimal scheduling, though market prices become higher during the next few hours. As shown in Fig. 6*b*, in most of the five scenarios, a large amount of electricity is sold in the day-ahead market in hours 16–20 due to high market prices during these periods. On 1 April and 18 August, the largest amount of electricity sold to the day-ahead market appears in hour 11. Since the power output of the PV plant on 18 August is the largest and market prices in the same day varies a bit from hours 11 to 21, the VPP operator is willing to sell the electricity in the day-ahead market rather than charge the battery fleets or sell it to the balancing market. Furthermore, the market price on 1 April has a sudden rise in hour 11, and thus nearly all the energy stored in the battery fleets during the previous 10 h is sold to the day-ahead market. Comparing Figs. 6*a* with b, the most significant difference is that electricity sold to the day-ahead market in case 1 varies less with market prices than that in case 2. Since the degradation cost is inevitable in case 1, the VPP operator opts to

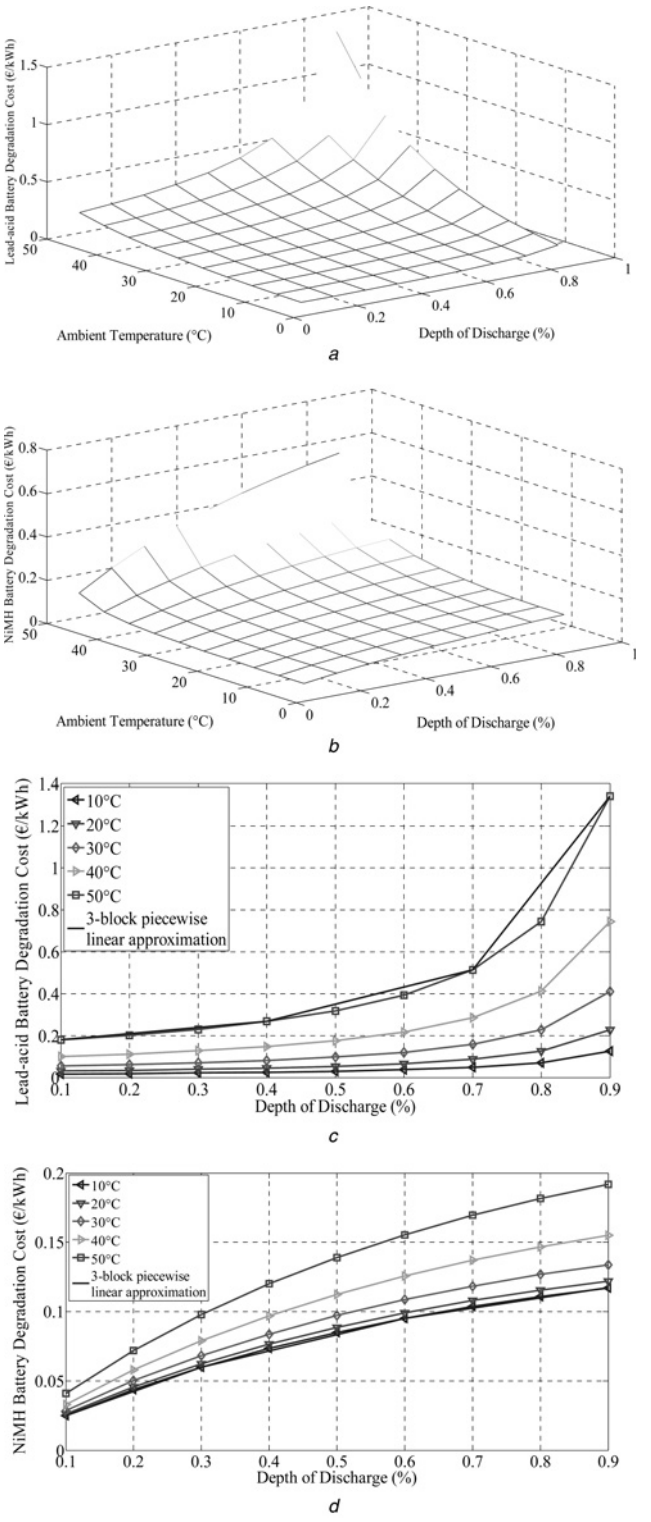

Fig. 4 *Correlations among degradation cost, ambient temperature, and DoD of the lead-acid battery and NiMH battery*

a Correlations among degradation cost, ambient temperature, and DoD of the lead-acid battery
b Correlations among degradation cost, ambient temperature, and DoD of the NiMH battery
c Correlation between degradation cost and DoD of the lead-acid battery under different ambient temperatures
d Correlation between degradation cost and DoD of the NiMH battery under different ambient temperatures

reduce the operation of the battery fleets, and utilise balancing market to sell/purchase more electricity to maximise the profit. Moreover, the results in the two figures indicate that electricity

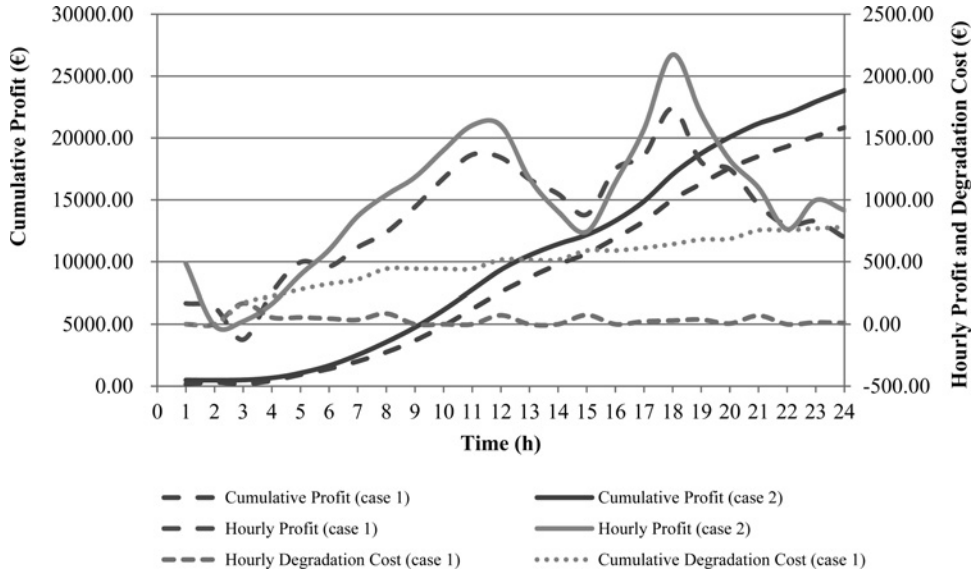

Fig. 5 *Expected hourly and cumulative profit of VPP together with the hourly and cumulative degradation cost in the two cases*

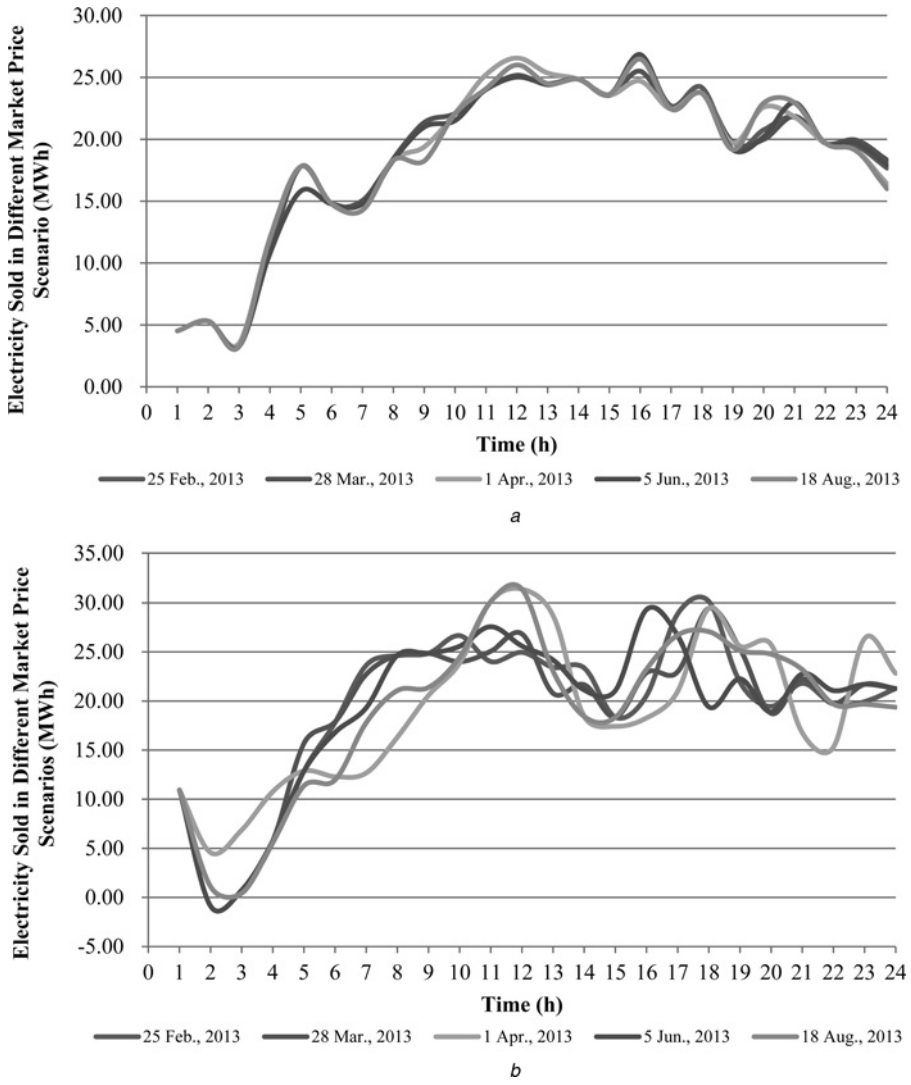

Fig. 6 *Electricity sold to the day-ahead market in different market price scenarios in the two cases*

a Electricity sold to the day-ahead market in different market price scenarios in case 1
b Electricity sold to the day-ahead market in different market price scenarios in case 2

sold to the day-ahead market is directly proportional with the market price. In other words, more electricity is sold when the market price is high, and less electricity is sold otherwise.

In order to thoroughly understand the effect of battery degradation cost on the optimal scheduling of the VPP, the following four scenarios in the two cases are simulated and analysed in detail:

(i) low variation of WPP and PV output, low day-ahead market prices;
(ii) low variation of WPP and PV output, high day-ahead market prices;
(iii) high variation of WPP and PV output, low day-ahead market prices;
(iv) high variation of WPP and PV output, high day-ahead market prices.

Assuming that in Figs. 7 and 8, a positive value of the day-ahead market curve indicates the electricity is sold, a positive value of the balancing market curve indicates electricity is purchased and a negative value of the battery fleet means it is charged. Besides, WPP, PV, and CTPP power output are always positive.

Figs. 7*a* and *b* show the optimal scheduling results of the VPP in the first simulation scenario for cases 1 and 2, respectively. A comparison between the two figures indicates that, in order to perform the offering commitments to the day-ahead market, extra electricity (43.63 MWh) is purchased by the VPP operator throughout the day in the balancing market in case 1. The CTPP in case 1 produces electricity at its full capacity during hours 10–23 while the CTPP in case 2 produces less electricity due to low day-ahead market prices. During the considered time horizon, the overall electricity sold to the day-ahead market is 355.26 MWh in case 1 while 231.95 MWh in case 2, which causes a significant reduction of profit in case 1 due to the low day-ahead market price scenario. Since battery degradation cost is counted in case 1, the VPP operator chooses to purchase electricity in the balancing market and schedule the CTPP generate more electricity to sell in the day-ahead market during periods of high prices instead of operating the battery fleets. In other words, the balancing market and CTPP perform like the ESS in case 1. The overall electricity flowing through the battery fleets in case 1 is 31.48 MW while in case 2 is 75.86 MW. This is because the VPP operator in case 1 tries to use the battery fleets as little as possible to reduce the degradation cost. In addition, battery fleet *a* in case 1 is not frequently used compared with battery fleet *b* since the degradation cost of lead-acid battery is higher than that of a NiMH battery.

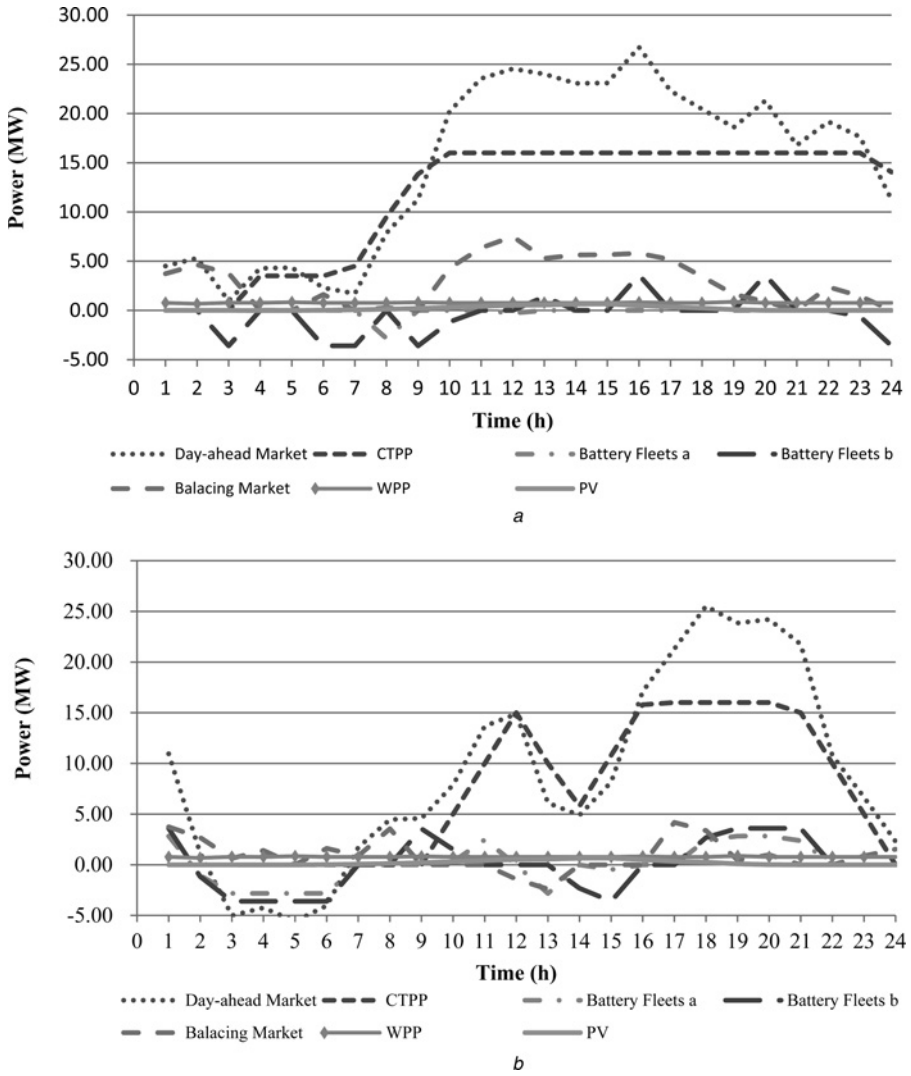

Fig. 7 *Optimal scheduling results of the VPP in the first and second simulation scenarios in the two cases*

a Optimal scheduling results of the VPP in the first simulation scenario in case 1
b Optimal scheduling results of the VPP in the first simulation scenario in case 2
c Optimal scheduling results of the VPP in the second simulation scenario in case 1
d Optimal scheduling results of the VPP in the second simulation scenario in case 2

IET Gener. Transm. Distrib., 2016, Vol. 10, Iss. 3, pp. 712–725

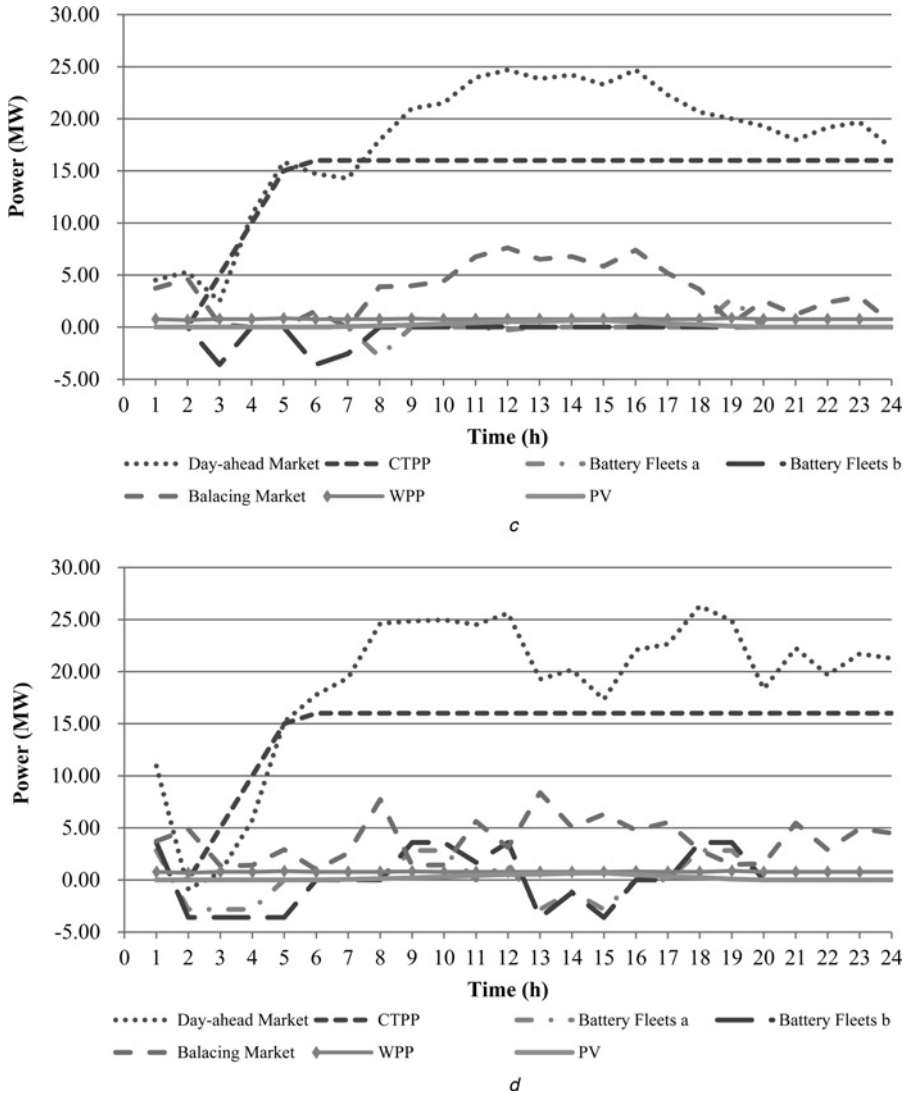

Fig. 7 *Continued*

The optimal scheduling results of the VPP in the second simulation scenario in cases 1 and 2 are presented in Figs. 7*c* and *d*, respectively. It can be seen from the two figures, a large amount of electricity is sold to the day-ahead market in both of the two cases because of the high market prices. The CTPP stays on-line all day long and generates electricity at its maximum capacity in order to accomplish the offering commitments. Electricity purchased in the balancing market during hours 1–3 and 5–24 in case 1 is only for selling in the day-ahead market. However, in case 2, a part of the electricity purchased in the balancing market is employed to charge the battery fleets for more profit. It is important to note that the electricity sold to the day-ahead market during periods of high market prices (hours 8–12 and 16–21) in case 2 is 249.02 MWh, nearly 58% of the total electricity sold to the day-ahead market. While in case 1, this percentage is 54%. This is because in case 2, battery fleets are charged in periods of low market prices and discharged in high market prices, while they are hardly discharged in case 1 for averting the degradation cost.

The results of the third simulation scenario are depicted in Figs. 8*a* and *b*. As shown in Fig. 8*a*, a large number of the WPP generations are sold to the balancing market, and the rest parts are either sold to the day-ahead market or used to charge the battery fleets. As mentioned before, selling electricity to the balancing market is less profitable than selling it to the day-ahead market. Nevertheless, since $G_{w,s,p,t}$ is independent of the WPP generation, the VPP operator is necessary to sell electricity to the balancing market rather than to the day-ahead market in some cases. Although the profit will be decreased in this scenario, the overall performance of the scheduling is optimum. Since battery fleets are seldom discharged in case 1, nearly all of the PV generations are sold to the day-head market and the CTPP is on-line for the whole day apart from hour 1 to fulfil offering commitments. As the result of degradation cost, the battery fleets are charged during hours 3, 6–10, but discharged only at hours 15–16. Comparing with case 1, the battery fleets in case 2 are more frequently operated to store electricity at periods of low market prices and sell it at high market prices with the purpose of optimised scheduling. Furthermore, the electricity sold to the balancing market in case 2 is less than case 1, which brings higher profit in case 2. The CTPP stays on-line only for 7 h in case 2 due to low day-head market prices.

Figs. 8*c* and *d* depict the results of the fourth simulation scenario. Due to high market prices, the electricity sold to the day-ahead market in the fourth simulation scenario is higher than that in the third simulation scenario in both cases 1 and 2, which reaches 429.35 and 450.28 MWh, respectively. The results in Fig. 8*c* indicate that the balancing market in case 1 is mainly used to tackle the imbalances between electricity production and electricity traded in the day-ahead market caused by the WPP and PV generations. While in case 2, the WPP and PV generations are utilised mostly for charging the battery fleets. Moreover, in order to reduce the degradation cost, battery fleets in case 1 are charged

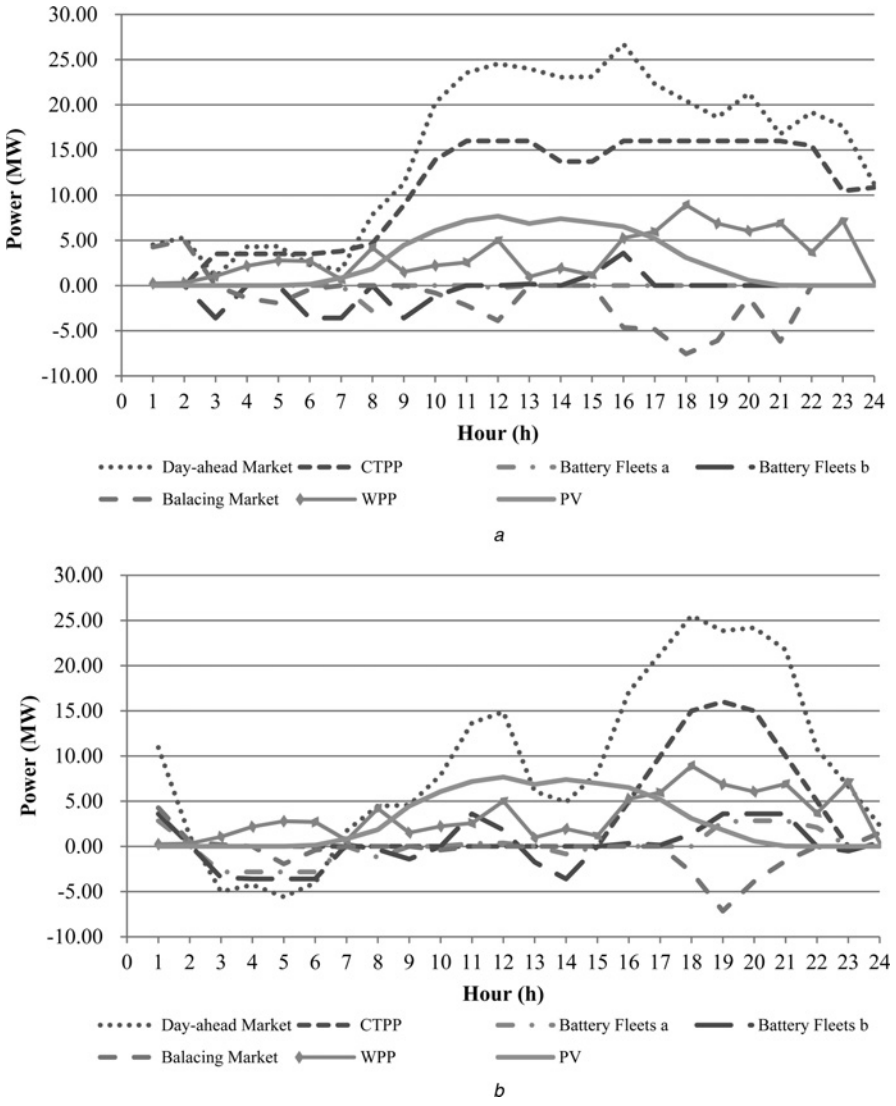

Fig. 8 *Optimal scheduling results of the VPP in the third and fourth simulation scenarios in the two cases*

a Optimal scheduling results of the VPP in the third simulation scenario in case 1
b Optimal scheduling results of the VPP in the third simulation scenario in case 2
c Optimal scheduling results of the VPP in the fourth simulation scenario in case 1
d Optimal scheduling results of the VPP in the fourth simulation scenario in case 2

during hours 3, 6–8, and 12, which exhibit the periods of low market prices, but discharged only a small amount of electricity (1.82 MWh) during period of high market prices (hour 19), though this brings a negative impact on the overall profit comparing with case 2. As a result of high day-ahead market prices, the CTPP in both of the two cases is running at its full capacity until hour 24.

The ambient temperature in the aforementioned two cases is assumed to be 20°C. However, in the real world, ambient temperature varies across a day and various areas. The expected profits of the VPP containing two types of battery fleets under different ambient temperatures are shown in Fig. 9. Battery fleets 1 contains 1000 lead-acid batteries and battery fleets 2 contains 1000 NiMH batteries. It is assumed that the initial energy storages of the two battery fleets are 2.83 and 3.6 MW, respectively. The results in Fig. 9 indicate that the expected profit decreases with the increase of ambient temperature, because with the same DoD, high ambient temperature causes high degradation cost for both lead-acid and NiMH batteries. Moreover, as a result of the logarithmical correlation between ambient temperature and degradation cost for lead-acid battery, when the ambient temperature increases, the expected profit of VPP containing battery fleets 1 has more reduction compared with the VPP containing battery fleets 2.

The above optimal scheduling results and expected profit are obtained from the risk-neutral model (11) without consideration of a risk measure. Nevertheless, due to the uncertainties in renewable generations and day-ahead market prices, the VPP agent has high risks associated with decisions trading in the electricity market. Therefore, the optimal scheduling decisions should hedge against these uncertainties to be more profitable while controlling the profit variability within a moderate range. In this paper, the CVaR at the α confidence level (CVaR_α) is used as the risk measure to assess and control the risk of the scheduling decisions, since it has good mathematical properties and can be readily included in the risk-neutral model. The CVaR is defined approximately as the expected profit of the $(1-\alpha)\cdot 100\%$ least profitable scenarios when it maximises a discrete profit distribution [13].

Consequently, the objective function with risk measure can be formulated as follows

$$\begin{aligned}\max & \sum_{t\in T}\sum_{w\in n_w}\pi_w\cdot\sum_{s\in n_s}\pi_s\cdot\sum_{p\in n_p}\pi_p \\ & \cdot[\lambda_{p,t}\cdot(G_{w,s,p,t}+g^{\mathrm{down}}_{w,s,p,t}\cdot\varphi_{\mathrm{down}}-g^{\mathrm{up}}_{w,s,p,t}\cdot\varphi_{\mathrm{up}}) \\ & -C^{\mathrm{C}}_{w,s,p,t}-y_{w,s,p,t}\cdot S_{\mathrm{c}}-C^{B}_{w,s,p,b,t}]+\beta\cdot\mathrm{CVaR}\end{aligned} \tag{30}$$

IET Gener. Transm. Distrib., 2016, Vol. 10, Iss. 3, pp. 712–725

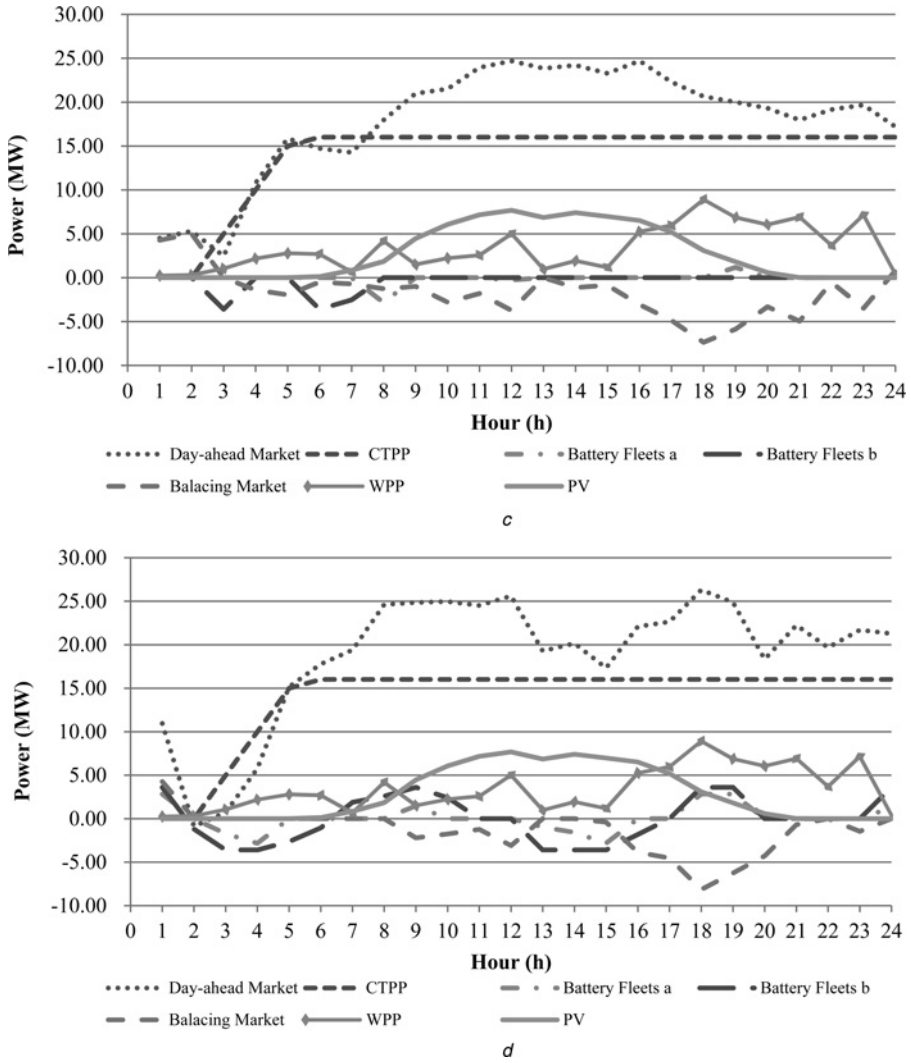

Fig. 8 *Continued*

subject to constraints (12)–(29) plus the following three constraints:

$$\mathrm{CVaR} = \zeta - \frac{1}{1-\alpha} \cdot \sum_{w \in n_w} \pi_w \cdot \sum_{s \in n_s} \pi_s \cdot \sum_{p \in n_p} \pi_p \cdot \eta_{w,s,p} \tag{31}$$

$$\zeta - \sum_{t \in T} [\lambda_{p,t} \cdot (G_{w,s,p,t} + g^{\mathrm{down}}_{w,s,p,t} \cdot \varphi_{\mathrm{down}} - g^{\mathrm{up}}_{w,s,p,t} \cdot \varphi_{\mathrm{up}}) - C^{\mathrm{C}}_{w,s,p,t} - y_{w,s,p,t} \cdot S_{\mathrm{c}} - C^{B}_{w,s,p,b,t}] \leq \eta_{w,s,p} \tag{32}$$

$$\forall w \in n_w, \forall s \in n_s, \forall p \in n_p$$

$$\eta_{w,s,p} \geq 0, \quad \forall w \in n_w, \forall s \in n_s, \forall p \in n_p \tag{33}$$

The objective function (30) includes the expected profit of the VPP and the weighted CVaR. Constraint (31) is used to calculate the CVaR. Constraints (32) and (33) are linear formulation of the CVaR. $\beta \in [0, \infty)$ is a weighting parameter used to define the tradeoff between expected profit and risk averse. If the risk is neglected, i.e. $\beta = 0$, the VPP scheduling model becomes a risk-neutral one. As the β increases, more risk averse will be considered by the VPP agent with regard to the expected profit.

By assuming $\beta = 0.4$and $\alpha = 95\%$, the expected daily profit of the VPP considering risk measure in case 1 is 19 722.86 €, which is lower than 20 839.87 € in the risk-neutral case ($\beta = 0$). This is because the CVaR aims to maximise the expected profit of the least profitable scenarios at the expense of a moderate reduction in the expected profit. In other words, the risk of experiencing profit distributions with high probability of low profit is controlled by the CVaR. Fig. 10 shows the efficient frontier, i.e. a collection of optimal points obtained for different values of β. As can be seen from Fig. 10, the CVaR increases significantly with a moderate reduction of expected profit when β increases. For example, a 37.6% increment of the CVaR indicates only a 6.9% reduction of the expected profit when β is increased from 0 to 0.5. Fig. 10 also shows that a small value of β yields the scheduling decisions with high expected profit and high risk while a large value of β

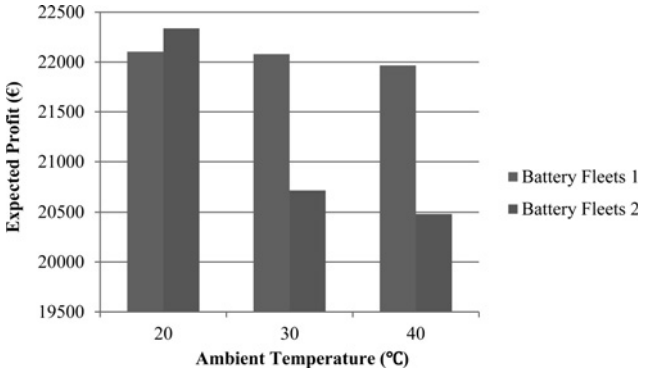

Fig. 9 *Expected profit of the VPP containing two types of battery fleets under different ambient temperatures*

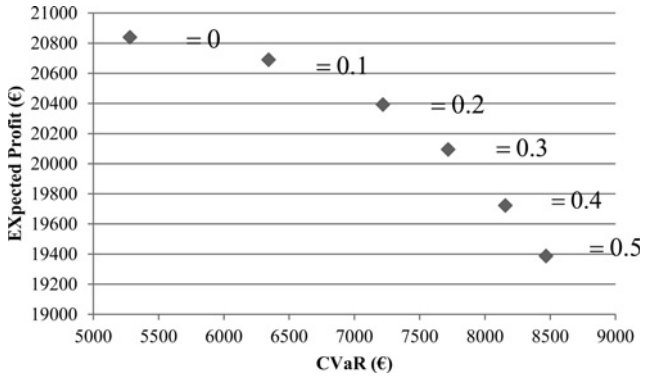

Fig. 10 *Efficient frontier*

Table 3 A comparison among the results obtained with different MILP solving algorithms

Algorithms	Computational time, s	Iterations	Gap, %	Objective
branch and cut	264.30	52,262	6.60	20839.8676
dynamic search	259.98	55,729	6.59	20839.8676
MILP heuristic	234.89	49,418	5.48	20839.8676
relaxation induced neighbourhood search heuristic	314.86	59,592	5.36	20839.8676

represents scheduling decisions with smaller expected profit and smaller risk.

The proposed model contains 102,121 variables (18,000 binaries) and 89,750 constraints, which is solved by IBM ILOG CPLEX Optimization Studio® Version 12.6 on a desktop with 3.40 GHz core i7 processor and 16.0 GB RAM. The overall computational time is about 3 min 54 s.

As a mathematic optimisation software package, CPLEX can efficiently solve linear programming problems, quadratic programming problems, mixed integer programming problems, quadratically constrained problems and so on. Although various evolutionary algorithms and stochastic search algorithms have been widely applied to solve the optimisation problems, these approaches have the disadvantages of time-consuming iterative computations and performance instability. The proposed VPP model is a large-scale MILP problem which cannot be efficiently solved by most of the intelligent heuristic algorithms. Therefore, the CPLEX is utilised to cope with the proposed MILP model. A comparison among the results obtained with different MILP solving algorithms is presented in Table 3.

As shown in Table 3, the optimised objective value of each algorithm is the same. Although the branch and cut algorithm is a high performance technique for solving various MILP problems, it suffers from relative high gap tolerance and long computational time compared with other algorithms. Among the four algorithms, MILP heuristic has the highest efficiency on the computational time, the fewest iterations and relative lower Gap. Hence, the MILP heuristic algorithm is used to solve the proposed VPP model in this paper.

4 Conclusions

In this paper, a two-stage stochastic MILP is developed to achieve the optimal scheduling for a VPP with battery degradation cost. Battery fleets including lead-acid and NiMH batteries are utilised as the ESS. Furthermore, DoD, and ambient temperature are used to model the battery degradation cost. Through the comprehensive analysis for the effects of degradation cost on optimal VPP scheduling and detailed comparison between the two cases, the following conclusions can be drawn:

(i) Electricity sold/purchased in the day-ahead market at each hour varies less with market prices. In other words, as a result of battery degradation cost, battery fleets are not frequently used to be charged or discharged.

(ii) In order to make profit, the CTPP is more committed even in case of low day-ahead market prices, since the fuel cost of CTPP is cheaper than the battery degradation cost. Therefore, more electricity is sold to the day-ahead market in case of low market prices.

(iii) Since the battery fleets are less operated, the VPP operator purchases more electricity in the balancing market and sold it to the day-ahead market in case of low variation of WPP and PV power outputs. Furthermore, with the high variation of WPP and PV generation outputs, the balancing market is mainly used to compensate the volatile generation.

(iv) The batteries with lower degradation cost are more dispatched by the VPP operator to reduce the degradation cost and maximise the overall expected profit.

(v) Higher ambient temperature causes lower expected profit and the reduction is related to the correlation between ambient temperature and degradation cost of the battery.

(vi) The risk measure can help VPP agent hedge against the uncertain renewable generations and market prices to achieve optimal scheduling of the VPP while controlling the profit variability within a moderate range.

5 Acknowledgments

The authors gratefully acknowledge the support of the International Science and Technology Cooperation Program of China under Grant 2012DFA70580, and the Fundamental Research Funds for the Central Universities.

6 References

1 Muñoz, C., Sauma, E., Contreras, J., *et al.*: 'Impact of high wind power penetration on transmission network expansion planning', *IET Gener. Transm. Distrib.*, 2012, **6**, (12), pp. 1281–1291
2 Garcia-Gonzalez, J., de la Muela, R.M.R., Santos, L.M., *et al.*: 'Stochastic joint optimization of wind generation and pumped-storage units in an electricity market', *IEEE Trans. Power Syst.*, 2008, **23**, (2), pp. 460–468
3 Vasirani, M., Kota, R., Cavalcante, R.L.G., *et al.*: 'An agent-based approach to virtual power plants of wind power generators and electric vehicles', *IEEE Trans. Smart Grid*, 2013, **4**, (3), pp. 1314–1322
4 Soroudi, A., Amraee, T.: 'Decision making under uncertainty in energy systems: State of the art', *Renew. Sustain. Energy Rev.*, 2013, **28**, pp. 376–384
5 Pudjianto, D., Ramsay, C., Strbac, G.: 'Virtual power plant and system integration of distributed energy resources', *IET Renew. Power Gener.*, 2007, **1**, (1), pp. 10–16
6 Matevosyan, J., Soder, L.: 'Minimization of imbalance cost trading wind power on the short-term power market', *IEEE Trans. Power Syst.*, 2006, **21**, (3), pp. 1396–1404
7 Yang, H., Yi, D., Zhao, J.: 'Distributed optimal dispatch of virtual power plant via limited communication', *IEEE Trans. Power Syst.*, 2013, **28**, (3), pp. 3511–3512
8 Petersen, M.K., Hansen, L.H., Bendtsen, J., *et al.*: 'Heuristic optimization for the discrete virtual power plant dispatch problem', *IEEE Trans. Smart Grid*, 2014, **5**, (6), pp. 2910–2918
9 Sousa, T., Morais, H., Soares, J., *et al.*: 'Day-ahead resource scheduling in smart grids considering Vehicle-to-Grid and network constraints', *APPL. Energy*, 2012, **96**, pp. 183–193
10 Pandžić, H., Morales, J.M., Conejo, A.J., *et al.*: 'Offering model for a virtual power plant based on stochastic programming', *APPL. Energy*, 2013, **105**, pp. 282–292
11 Pandžić, H., Kuzle, I., Capuder, T.: 'Virtual power plant mid-term dispatch optimization', *APPL. Energy*, 2013, **101**, pp. 134–141
12 Tajeddini, M.A., Rahimi-Kian, A., Soroudi, A.: 'Risk averse optimal operation of a virtual power plant using two stage stochastic programming', *Energy*, 2014, **73**, pp. 958–967
13 Al-Awami, A.T., El-Sharkawi, M.A.: 'Coordinated trading of wind and thermal energy', *IEEE Trans. Sustain. Energy*, 2011, **2**, (3), pp. 277–287
14 Vasirani, M., Kota, R., Cavalcante, R.L.G., *et al.*: 'An agent-based approach to virtual power plants of wind power generators and electric vehicles', *IEEE Trans. Smart Grid*, 2013, **4**, (3), pp. 1314–1322
15 Arslan, O., Karasan, O.E.: 'Cost and emission impacts of virtual power plant formation in plug-in hybrid electric vehicle penetrated networks', *Energy*, 2013, **60**, pp. 116–124
16 Amiri, M., Esfahanian, M., Hairi-Yazdi, M.R., *et al.*: 'Minimization of power losses in hybrid electric vehicles in view of the prolonging of battery life', *J. Power Sources*, 2009, **190**, (2), pp. 372–379

17 Zhou, C., Qian, K., Allan, M., *et al*.: 'Modeling of the cost of EV battery wear due to V2G application in power systems', *IEEE Trans. Energy Convers.*, 2011, **26**, (4), pp. 1041–1050
18 Evans, A., Strezov, V., Evans, T.J.: 'Assessment of utility energy storage options for increased renewable energy penetration', *Renew. Sustain. Energy Rev.*, 2012, **16**, (6), pp. 4141–4147
19 Carter, R., Cruden, A., Hall, P.J.: 'Optimizing for efficiency or battery life in a battery/supercapacitor electric vehicle', *IEEE Trans. Veh. Technol.*, 2012, **61**, (4), pp. 1526–1533
20 Schaltz, E., Khaligh, A., Rasmussen, P.O.: 'Influence of battery/ultracapacitor energy-storage sizing on battery lifetime in a fuel cell hybrid electric vehicle', *IEEE Trans. Veh. Technol.*, 2009, **58**, (8), pp. 3882–3891
21 Elattar, E.E.: 'Prediction of wind power based on evolutionary optimised local general regression neural network', *IET Gener. Transm. Distrib.*, 2014, **8**, (5), pp. 916–923
22 El-Fouly, T.H.M., El-Saadany, E.F., Salama, M.M.A.: 'Improved Grey predictor rolling models for wind power prediction', *IET Gener. Transm. Distrib.*, 2007, **1**, (6), pp. 928–937
23 Jafarzadeh, S., Fadali, M.S., Evrenosoglu, C.Y.: 'Solar power prediction using interval type-2 TSK modeling', *IEEE Trans. Sustain. Energy*, 2013, **4**, (2), pp. 333–339
24 Pindoriya, N.M., Singh, S.N., Singh, S.K.: 'An adaptive wavelet neural network-based energy price forecasting in electricity markets', *IEEE Trans. Power Syst.*, 2008, **23**, (3), pp. 1423–1432
25 Chen, J., Deng, S.-J., Huo, X.: 'Electricity price curve modeling and forecasting by manifold learning', *IEEE Trans. Power Syst.*, 2008, **23**, (3), pp. 877–888
26 Mohammadi, S., Mozafari, B., Solymani, S., *et al*.: 'Stochastic scenario-based model and investigating size of energy storages for PEM-fuel cell unit commitment of micro-grid considering profitable strategies', *IET Gener. Transm. Distrib.*, 2014, **8**, (7), pp. 1228–1243
27 Tan, Y., Cao, Y., Li, C., *et al*.: 'A two-stage stochastic programming approach considering risk level for distribution networks operation with wind power', *IEEE Syst. J.*, 2014, DOI: http://dx.doi.org/10.1109/JSYST.2014.2350027
28 Kempton, W., Tomić, J.: 'Vehicle-to-grid power fundamentals: calculating capacity and net revenue', *J. Power Sources*, 2005, **144**, (1), pp. 268–279
29 Swierczynski, M., Stroe, D.I., Stan, A.-I., *et al*.: 'Selection and performance-degradation modeling of $LiMO_2/Li_4Ti_5O_{12}$ and $LiFePO_4$/C battery cells as suitable energy storage systems for grid integration with wind power plants: an example for the primary frequency regulation service', *IEEE Trans. Sustain. Energy*, 2014, **5**, (1), pp. 90–101
30 Hoke, A., Brissette, A., Smith, K., *et al*.: 'Accounting for lithium-ion battery degradation in electric vehicle charging optimization', *IEEE J. Emerg. Sel. Top. Power Electron.*, 2014, **2**, (3), pp. 691–700
31 Han, S., Han, S.: 'Economic feasibility of V2G frequency regulation in consideration of battery wear', *Energies*, 2013, **6**, (2), pp. 748–765
32 'Actual solar power generation', http://www.transparency.eex.com/en/Statutory%20Publication%20Requirements%20of%20the%20Transmission%20System%20Operators/Power%20generation/Actual%20solar%20power%20generation#, accessed 15 December 2014
33 'UKPX auction historical data', http://www.apxgroup.com/market-results/apx-power-uk/ukpx-auction-historical-data/, accessed 20 December 2014